

Theoretical Uncertainties in Inflationary Predictions

William H. Kinney*

Dept. of Physics, University at Buffalo, the State University of New York, Buffalo, NY 14260-1500

Antonio Riotto†

CERN, Theory Division, CH-1211 Geneva 23, Switzerland

(Dated: October 31, 2018)

With present and future observations becoming of higher and higher quality, it is timely and necessary to investigate the most significant theoretical uncertainties in the predictions of inflation. We show that our ignorance of the entire history of the Universe, including the physics of reheating after inflation, translates to considerable errors in observationally relevant parameters. Using the inflationary flow formalism, we estimate that for a spectral index n and tensor/scalar ratio r in the region favored by current observational constraints, the theoretical errors are of order $\Delta n / |n - 1| \sim 0.1 - 1$ and $\Delta r / r \sim 0.1 - 1$. These errors represent the dominant theoretical uncertainties in the predictions of inflation, and are generically of the order of or larger than the projected uncertainties in future precision measurements of the Cosmic Microwave Background. We also show that the lowest-order classification of models into small field, large field, and hybrid breaks down when higher order corrections to the dynamics are included. Models can flow from one region to another.

PACS numbers: 98.80.Cq

I. INTRODUCTION

Inflation [1] has become the dominant paradigm for understanding the initial conditions for structure formation and for Cosmic Microwave Background (CMB) anisotropies. In the inflationary picture, primordial density and gravitational-wave fluctuations are created from quantum fluctuations, “redshifted” beyond the horizon during an early period of superluminal expansion of the universe, then “frozen” [2, 3, 4]. Perturbations at the surface of last scattering are observable as temperature anisotropies in the CMB, as first detected by the Cosmic Background Explorer satellite [5, 6]. The latest and most impressive confirmation of the inflationary paradigm has been recently provided by data from the Wilkinson Microwave Anisotropy Probe (WMAP) satellite, which marks the beginning of the precision era of CMB measurements in space [7]. The WMAP collaboration has produced a full-sky map of the angular variations of the CMB to unprecedented accuracy. WMAP data support the inflationary mechanism as the mechanism for the generation of super-horizon curvature fluctuations.

The CMB contains a wealth of information about the properties of the spectrum of primeval density perturbations and present data already allow to extract relevant informations about the parameters of single-field models of inflation [8], *i.e.* models whose inflation is driven by one scalar field, the inflaton. The following parameters have been identified as important for accurately computing the expected anisotropy and for discriminat-

ing among different inflationary models: the power-law indices of the scalar and tensor perturbations n and n_T respectively and the tensor-to-scalar amplitude ratio $r = 16(P_T/P_R)$. Present data are consistent with a scale-invariant spectrum of scalar perturbation ($n = 1$) and with an amount of tensor perturbations such that $r \lesssim 0.5$ [8]. However, future CMB experiments will allow an accurate determination of the properties the scalar spectrum. The satellite-borne experiment Planck [9], the proposed high-resolution version of CMBpol [10] and a polarized bolometer array on the South Pole Telescope [11] will allow a determination of the spectral index n with a standard deviation of about 0.007, 0.003 and 0.01, respectively [12]. At the same time a positive detection of the tensor modes through the B -mode of CMB polarization (once foregrounds due to gravitational lensing from local sources have been properly treated) requires $r \gtrsim 10^{-3}$ [13]. While this limit is below the expected sensitivity, a tensor to scalar ratio of $r \sim 0.01$ is well within the reach of presently feasible CMB observations. The proposed Big Bang Observer satellite has the potential to probe $r \sim 0.001$ [14].

With present and future observations reaching a higher and higher quality, it becomes timely and necessary to investigate the most significant uncertainties on the theoretical side as far as inflationary predictions are concerned. In this paper we study the impact of our ignorance about the precise location on the inflationary potential corresponding to the observed perturbations. This is quantified by the number of e -foldings N before the end of inflation at which our present Hubble scale equalled the Hubble scale during inflation, the so-called epoch of horizon-crossing. Indeed, the determination of the number of e -foldings requires the knowledge of the entire history of the Universe. The expression for N can be written as

*Electronic address: whkinney@buffalo.edu

†Electronic address: antonio.riotto@pd.infn.it

$$N \simeq 60 + \frac{1}{6} \ln(-n_T) + \frac{1}{3} \ln(T_{\text{RH}}/10^{16} \text{ GeV}) - \frac{1}{3} \ln \gamma, \quad (1)$$

where T_{RH} is the reheating temperature, γ is the ratio of the entropy per comoving volume today to that after reheating and quantifies any post-inflation entropy production and we have assumed that there is no significant drop in energy density during the last stages of inflation. The main uncertainties in the determination of the number of e -foldings are caused by our ignorance about the last two terms. The reheating temperature T_{RH} after inflation may vary from the Grand Unified Theory scale $\sim 10^{16}$ GeV to 1 MeV, the scale at which nucleosynthesis takes place. In this range, the corresponding shift of N is about 14. Furthermore, long-lived massive particles of mass of the order of the weak scale are ubiquitous in string-inspired models (they are generically dubbed moduli) and may dominate the energy density of the Universe after reheating, leading to a prolonged matter-dominated epoch followed by a large amount of entropy release at the time of moduli decay [15], $\gamma \gg 1$. The corresponding shift in the number of *folding*s can be as large as 10. One can even envisage extreme situations where the reduction of the energy scale during inflation is so significant that the shift in N is as large as 70 [16].

Given the fact that the values of the inflationary observables n , n_T and r are evaluated at the value of N corresponding to the moment when the present Hubble scale crossed outside the horizon during inflation and that such a value is affected by a non-negligible uncertainty, we immediately conclude that the predictions of the inflationary observables are affected by unavoidable theoretical errors. How can we quantify them? Are they larger or smaller than the expected accuracy of forthcoming experiments? We propose to use the method of “flow” to gain some insight. The flow equations provide the derivatives of the inflationary observables with respect to the number of e -foldings as a function of the observable themselves at any order in the so-called slow-roll parameters [17, 18, 19]. For instance, to lowest order in slow roll

$$\begin{aligned} \frac{dr}{dN} &= r \left[(n-1) + \frac{r}{8} \right], \\ \frac{dn}{dN} &= -\frac{5}{16} r(n-1) - \frac{3}{32} r^2 + 2\xi^2, \end{aligned} \quad (2)$$

where $\xi^2 \equiv (m_{\text{Pl}}^4/16\pi^2) (H'H'''/H^2)$, m_{Pl} being the Planck scale, H the Hubble rate during inflation and primes indicate differentiation with respect to the inflaton field. From this set of equations we can easily quantify – within any given single-field model of inflation – how our ignorance on the precise value of the number of e -foldings ΔN , is reflected in the predicted value of the observable quantities. The expected uncertainties are model-dependent, but roughly speaking, we expect a theoretical error of the magnitude $\Delta r \sim (dr/dN)_* \Delta N$

and $\Delta n \sim (dn/dN)_* \Delta N$, where the derivatives are evaluated at a reference number of e -folding, *e.g.* at $N_* \sim 60$ corresponding to $T_{\text{RH}} \sim 10^{16}$ GeV and $\gamma \sim 1$ and $\Delta N = (N - N_*)$. We conclude that – generically – the error in the tensor-to-scalar ratio is of order $\Delta r/r \sim 0.1 - 1$, and the error in the spectral index is of order $\Delta n/|n-1| \sim 0.1 - 1$ (for $\Delta N \sim 14$). These errors are of the order of or larger than the accuracy expected from future experiments.

The paper is organized as follows. In Sec. II we discuss single-field inflation and the relevant observables in more detail. In Sec. III we discuss the inflationary model space, and in Sec. IV we describe the flow technique to quantify the theoretical errors in the inflationary predictions. In Sec. V we present our results and offer some analytical explanations. Finally, in Sec. VI we present our conclusions.

II. SINGLE-FIELD INFLATION AND THE INFLATIONARY OBSERVABLES

In this section we briefly review scalar field models of inflationary cosmology, and explain how we relate model parameters to observable quantities. Inflation, in its most general sense, can be defined to be a period of accelerating cosmological expansion during which the universe evolves toward homogeneity and flatness. This acceleration is typically a result of the universe being dominated by vacuum energy, with an equation of state $p \simeq -\rho$. Within this broad framework, many specific models for inflation have been proposed. We limit ourselves here to models with “normal” gravity (*i.e.*, general relativity) and a single order parameter for the vacuum, described by a slowly rolling scalar field ϕ , the inflaton.

A scalar field in a cosmological background evolves with an equation of motion

$$\ddot{\phi} + 3H\dot{\phi} + V'(\phi) = 0. \quad (3)$$

The evolution of the scale factor is given by the scalar field dominated FRW equation,

$$\begin{aligned} H^2 &= \frac{8\pi}{3m_{\text{Pl}}^2} \left[\frac{1}{2}\dot{\phi}^2 + V(\phi) \right], \\ \left(\frac{\ddot{a}}{a} \right) &= \frac{8\pi}{3m_{\text{Pl}}^2} \left[V(\phi) - \dot{\phi}^2 \right]. \end{aligned} \quad (4)$$

We have assumed a flat Friedmann-Robertson-Walker metric,

$$g_{\mu\nu} = \text{diag}(1, -a^2, -a^2 - a^2), \quad (5)$$

where $a^2(t)$ is the scale factor of the universe. *Inflation* is defined to be a period of accelerated expansion, $\ddot{a} > 0$. A powerful way of describing the dynamics of a scalar field-dominated cosmology is to express the Hubble parameter as a function of the field ϕ , $H = H(\phi)$, which is consistent

provided ϕ is monotonic in time. The equations of motion become [20, 21, 22, 23]:

$$\begin{aligned}\dot{\phi} &= -\frac{m_{\text{Pl}}^2}{4\pi} H'(\phi), \\ [H'(\phi)]^2 - \frac{12\pi}{m_{\text{Pl}}^2} H^2(\phi) &= -\frac{32\pi^2}{m_{\text{Pl}}^4} V(\phi).\end{aligned}\quad (6)$$

These are completely equivalent to the second-order equation of motion in Eq. (3). The second of the above equations is referred to as the *Hamilton-Jacobi* equation, and can be written in the useful form

$$H^2(\phi) \left[1 - \frac{1}{3}\epsilon(\phi) \right] = \left(\frac{8\pi}{3m_{\text{Pl}}^2} \right) V(\phi), \quad (7)$$

where ϵ is defined to be

$$\epsilon \equiv \frac{m_{\text{Pl}}^2}{4\pi} \left(\frac{H'(\phi)}{H(\phi)} \right)^2. \quad (8)$$

The physical meaning of ϵ can be seen by expressing Eq. (4) as

$$\left(\frac{\ddot{a}}{a} \right) = H^2(\phi) [1 - \epsilon(\phi)], \quad (9)$$

so that the condition for inflation $(\ddot{a}/a) > 0$ is given by $\epsilon < 1$. The scale factor is given by

$$a \propto e^N = \exp \left[\int_{t_0}^t H dt \right], \quad (10)$$

where the number of *e*-folds N is

$$N \equiv \int_t^{t_e} H dt = \int_{\phi}^{\phi_e} \frac{H}{\dot{\phi}} d\phi = \frac{2\sqrt{\pi}}{m_{\text{Pl}}} \int_{\phi_e}^{\phi} \frac{d\phi}{\sqrt{\epsilon(\phi)}}. \quad (11)$$

whose value has been discussed in the Introduction.

We will frequently work within the context of the *slow roll* approximation which is the assumption that the evolution of the field is dominated by drag from the cosmological expansion, so that $\ddot{\phi} \simeq 0$ and

$$\dot{\phi} \simeq -\frac{V'}{3H}. \quad (12)$$

The equation of state of the scalar field is dominated by the potential, so that $p \simeq -\rho$, and the expansion rate is approximately

$$H \simeq \sqrt{\frac{8\pi}{3m_{\text{Pl}}^2} V(\phi)}. \quad (13)$$

The slow roll approximation is consistent if both the slope and curvature of the potential are small, $V', V'' \ll V$. In this case the parameter ϵ can be expressed in terms of the potential as

$$\epsilon \equiv \frac{m_{\text{Pl}}^2}{4\pi} \left(\frac{H'(\phi)}{H(\phi)} \right)^2 \simeq \frac{m_{\text{Pl}}^2}{16\pi} \left(\frac{V'(\phi)}{V(\phi)} \right)^2. \quad (14)$$

We will also define a second “slow roll parameter” η by:

$$\begin{aligned}\eta(\phi) &\equiv \frac{m_{\text{Pl}}^2}{4\pi} \left(\frac{H''(\phi)}{H(\phi)} \right) \\ &\simeq \frac{m_{\text{Pl}}^2}{8\pi} \left[\frac{V''(\phi)}{V(\phi)} - \frac{1}{2} \left(\frac{V'(\phi)}{V(\phi)} \right)^2 \right].\end{aligned}\quad (15)$$

Slow roll is then a consistent approximation for $\epsilon, \eta \ll 1$.

Inflation models not only explain the large-scale homogeneity of the universe, but also provide a mechanism for explaining the observed level of *inhomogeneity* as well. During inflation, quantum fluctuations on small scales are quickly redshifted to scales much larger than the horizon size, where they are “frozen” as perturbations in the background metric. The metric perturbations created during inflation are of two types: scalar, or *curvature* perturbations, which couple to the stress-energy of matter in the universe and form the “seeds” for structure formation, and tensor, or gravitational wave perturbations, which do not couple to matter. Both scalar and tensor perturbations contribute to CMB anisotropy. Scalar fluctuations can also be interpreted as fluctuations in the density of the matter in the universe. Scalar fluctuations can be quantitatively characterized by the comoving curvature perturbation $P_{\mathcal{R}}$. As long as the equation of state ϵ is slowly varying, the curvature perturbation can be shown to be [1]

$$P_{\mathcal{R}}^{1/2}(k) = \left(\frac{H^2}{2\pi\dot{\phi}} \right)_{k=aH} = \left[\frac{H}{m_{\text{Pl}}} \frac{1}{\sqrt{\pi\epsilon}} \right]_{k=aH}. \quad (16)$$

The fluctuation power spectrum is in general a function of wavenumber k , and is evaluated when a given mode crosses outside the horizon during inflation, $k = aH$. Outside the horizon, modes do not evolve, so the amplitude of the mode when it crosses back *inside* the horizon during a later radiation- or matter-dominated epoch is just its value when it left the horizon during inflation. Instead of specifying the fluctuation amplitude directly as a function of k , it is convenient to specify it as a function of the number of *e*-folds N before the end of inflation at which a mode crossed outside the horizon.

The *spectral index* n for $P_{\mathcal{R}}$ is defined by

$$n - 1 \equiv \frac{d \ln P_{\mathcal{R}}}{d \ln k}, \quad (17)$$

so that a scale-invariant spectrum, in which modes have constant amplitude at horizon crossing, is characterized by $n = 1$.

The power spectrum of tensor fluctuation modes is given by [1]

$$P_T^{1/2}(k_N) = \left[\frac{4H}{m_{\text{Pl}}\sqrt{\pi}} \right]_N. \quad (18)$$

The ratio of tensor-to-scalar modes is then

$$\frac{P_T}{P_{\mathcal{R}}} = 16\epsilon, \quad (19)$$

so that tensor modes are negligible for $\epsilon \ll 1$.

III. THE INFLATIONARY MODEL SPACE

To summarize the results of the previous section, inflation generates scalar (density) and tensor (gravity wave) fluctuations which are generally well approximated by power laws:

$$P_{\mathcal{R}}(k) \propto k^{n-1}; \quad P_T(k) \propto k^{n_T}. \quad (20)$$

In the limit of slow roll, the spectral indices n and n_T vary slowly or not at all with scale. We can write the spectral indices n and n_T to lowest order in terms of the slow roll parameters ϵ and η as:

$$\begin{aligned} n &\simeq 1 - 4\epsilon + 2\eta, \\ n_T &\simeq -2\epsilon. \end{aligned} \quad (21)$$

The tensor/scalar ratio is frequently expressed as a quantity r which is conventionally normalized as

$$r \equiv 16\epsilon = \frac{P_T}{P_{\mathcal{R}}} \quad (22)$$

The tensor spectral index is *not* an independent parameter, but is proportional to the tensor/scalar ratio, given to lowest order in slow roll by

$$n_T \simeq -2\epsilon = -\frac{r}{8}. \quad (23)$$

This is known as the *consistency relation* for inflation. A given inflation model can therefore be described to lowest order in slow roll by three independent parameters, $P_{\mathcal{R}}$, P_T , and n . If we wish to include higher-order effects, we have a fourth parameter describing the running of the scalar spectral index, $dn/d\ln k$.

Calculating the CMB fluctuations from a particular inflationary model reduces to the following basic steps: (1) from the potential, calculate ϵ and η . (2) From ϵ , calculate N as a function of the field ϕ . (3) Invert $N(\phi)$ to find ϕ_N . (4) Calculate $P_{\mathcal{R}}$, n , and P_T as functions of ϕ , and evaluate them at $\phi = \phi_N$. For the remainder of the paper, all parameters are assumed to be evaluated at $\phi = \phi_N$.

Even restricting ourselves to a simple single-field inflation scenario, the number of models available to choose from is large [1]. It is convenient to define a general classification scheme, or “zoology” for models of inflation. We divide models into three general types: *large-field*, *small-field*, and *hybrid*, with a fourth classification, *linear* models, serving as a boundary between large- and small-field. A generic single-field potential can be characterized by two independent mass scales: a “height” Λ^4 , corresponding to the vacuum energy density during inflation, and a “width” μ , corresponding to the change in the field value $\Delta\phi$ during inflation:

$$V(\phi) = \Lambda^4 f\left(\frac{\phi}{\mu}\right). \quad (24)$$

Different models have different forms for the function f . The height Λ is fixed by normalization, so the only free parameter is the width μ .

With the normalization fixed, the relevant parameter space for distinguishing between inflation models to lowest order in slow roll is then the $r - n$ plane. (To next order in slow-roll parameters, one must introduce the running of n .) Different classes of models are distinguished by the value of the second derivative of the potential, or, equivalently, by the relationship between the values of the slow-roll parameters ϵ and η . Each class of models has a different relationship between r and n . For a more detailed discussion of these relations, the reader is referred to Refs. [24, 25].

First order in ϵ and η is sufficiently accurate for the purposes of this Section, and for the remainder of this Section we will only work to first order. The generalization to higher order in slow roll will be discussed in the following.

A. Large-field models: $-\epsilon < \eta \leq \epsilon$

Large-field models have inflaton potentials typical of “chaotic” inflation scenarios [26], in which the scalar field is displaced from the minimum of the potential by an amount usually of order the Planck mass. Such models are characterized by $V''(\phi) > 0$, and $-\epsilon < \eta \leq \epsilon$. The generic large-field potentials we consider are polynomial potentials $V(\phi) = \Lambda^4 (\phi/\mu)^p$, and exponential potentials, $V(\phi) = \Lambda^4 \exp(\phi/\mu)$.

For the case of an exponential potential, $V(\phi) \propto \exp(\phi/\mu)$, the tensor/scalar ratio r is simply related to the spectral index as

$$r = 8(1 - n), \quad (25)$$

but the slow roll parameters are constant (there is no dependence upon N) and therefore no intrinsic errors of the observables n and r are expected in such a case.

For inflation with a polynomial potential, $V(\phi) \propto \phi^p$, we have

$$\begin{aligned} n - 1 &= -\frac{2 + p}{2N}, \\ r &= \frac{8p}{2N} = 8\left(\frac{p}{p + 2}\right)(1 - n), \end{aligned} \quad (26)$$

so that tensor modes are large for significantly tilted spectra. By shifting the number of *e*-foldings by ΔN one therefore expects

$$\frac{\Delta(n - 1)}{n - 1} = \frac{\Delta r}{r} = -\frac{\Delta N}{N}. \quad (27)$$

From these relations we deduce that sizeable correlated theoretical errors should be expected for those large-field models characterized by large deviations from a flat spectrum and by large values of the tensor-to-scalar amplitude ratio. Furthermore these errors increase with the

potential of the polynomial p . Of course, these statements are based on relations valid only at first order in the slow roll parameters. This means that for very large values of $(n - 1)$ and r higher order corrections become relevant and may significantly alter the simple relations (27).

B. Small-field models: $\eta < -\epsilon$

Small-field models are the type of potentials that arise naturally from spontaneous symmetry breaking (such as the original models of “new” inflation [27, 28]) and from pseudo Nambu-Goldstone modes (natural inflation [29]). The field starts from near an unstable equilibrium (taken to be at the origin) and rolls down the potential to a stable minimum. Small-field models are characterized by $V''(\phi) < 0$ and $\eta < -\epsilon$. Typically ϵ (and hence the tensor amplitude) is close to zero in small-field models. The generic small-field potentials we consider are of the form $V(\phi) = \Lambda^4 [1 - (\phi/\mu)^p]$, which can be viewed as a lowest-order Taylor expansion of an arbitrary potential about the origin. The cases $p = 2$ and $p > 2$ have very different behavior. For $p = 2$, $n - 1 \simeq -(1/2\pi)(m_{\text{Pl}}/\mu)^2$ and there is no dependence upon the number of e -foldings. On the other hand

$$r = 8(1 - n) \exp[-1 - N(1 - n)], \quad (28)$$

leading to

$$\frac{\Delta r}{r} = (n - 1)\Delta N. \quad (29)$$

For $p > 2$, the scalar spectral index is

$$n \simeq 1 - \frac{2}{N} \left(\frac{p-1}{p-2} \right), \quad (30)$$

independent of (m_{Pl}/μ) . Assuming $\mu < m_{\text{Pl}}$ results in an upper bound on r of

$$r < 8 \frac{p}{N(p-2)} \left(\frac{8\pi}{Np(p-2)} \right)^{p/(p-2)}. \quad (31)$$

The corresponding theoretical errors read

$$\begin{aligned} \frac{\Delta(n-1)}{n-1} &= -\frac{\Delta N}{N}, \\ \frac{\Delta r}{r} &\simeq (n-1)\Delta N \simeq -\frac{2(p-1)}{p-2} \frac{\Delta N}{N}. \end{aligned} \quad (32)$$

Due to the tiny predicted values of r , for small field models one expects generically tiny errors in the tensor-to-scalar amplitude ratio, but sizeable errors in the spectral index.

C. Hybrid models: $0 < \epsilon < \eta$

The hybrid scenario [30, 31, 32] frequently appears in models which incorporate inflation into supersymmetry. In a typical hybrid inflation model, the scalar field responsible for inflation evolves toward a minimum with nonzero vacuum energy. The end of inflation arises as a result of instability in a second field. Such models are characterized by $V''(\phi) > 0$ and $0 < \epsilon < \eta$. We consider generic potentials for hybrid inflation of the form $V(\phi) = \Lambda^4 [1 + (\phi/\mu)^p]$. The field value at the end of inflation is determined by some other physics, so there is a second free parameter characterizing the models. Because of this extra freedom, hybrid models fill a broad region in the $r - n$ plane. For $(\phi_N/\mu) \gg 1$ (where ϕ_N is the value of the inflaton field when there are e -foldings till the end of inflation) one recovers the same results of the large field models. On the contrary, when $(\phi_N/\mu) \ll 1$, the dynamics are analogous to small-field models, except that the field is evolving toward, rather than away from, a dynamical fixed point. This distinction is important to the discussion here because near the fixed point the parameters r and n become independent of the number of e -folds N , and the corresponding theoretical uncertainties due to the uncertainty in N vanish. However, there is an additional degree of freedom not present in other models due to the presence of the additional parameter ϕ_c . Therefore the theoretical uncertainties in the predictions of a generic hybrid inflation model are decoupled from the physics of reheating, and we do not consider such models further here. The distinguishing observational feature of many hybrid models is $\eta > 0$ and a *blue* scalar spectral index, $n > 1$.

Notice that at first order in the slow roll parameters, there is no overlap in the $r - n$ plane between hybrid inflation and other models. However, as we will explicitly show, this feature is lost going beyond first order: by changing N models can flow from the hybrid regions to other model regions; this feature is generic, models can flow from one region to another. Therefore it is important to distinguish between models labeled “hybrid” in the sense of evolution toward a late-time asymptote and the *region* labeled “hybrid” in the zoo plot. The lowest-order correspondence does not always survive to higher order in slow roll.

D. Linear models: $\eta = -\epsilon$

Linear models, $V(\phi) \propto \phi$, live on the boundary between large-field and small-field models, with $V''(\phi) = 0$ and $\eta = -\epsilon$. The spectral index and tensor/scalar ratio are related as:

$$r = \frac{8}{3}(1 - n). \quad (33)$$

For linear models, Eq. (27) applies.

This enumeration of models is certainly not exhaustive. There are a number of single-field models that do not fit well into this scheme, for example logarithmic potentials $V(\phi) = V_0 [1 + (Cg^2/8\pi) \ln(\phi/\mu)]$ typical of supersymmetry [1], where C counts the degrees of freedom coupled to the inflaton field and g is a coupling constant. For this kind of potentials, one gets $n - 1 \simeq -(1/N)$ and $r \simeq (2Cg^2/\pi^2)(1/N)$ corresponding to

$$\frac{\Delta(n-1)}{n-1} = \frac{\Delta r}{r} = -\frac{\Delta N}{N}. \quad (34)$$

Because of the loop-factor suppression, one typically expects tiny theoretical errors in r , but sizeable uncertainties in $n - 1$.

Another example is potentials with negative powers of the scalar field $V(\phi) = V_0 [1 + \alpha(m_{\text{Pl}}/\phi)^p]$ used in intermediate inflation [33] and dynamical supersymmetric inflation [34, 35]. Both of these cases require an auxiliary field to end inflation and are more properly categorized as hybrid models, but fall into the small-field region of the $r - n$ plane. The power spectrum is blue being the spectral index given by $n - 1 \simeq 2(p + 1/p + 2)(2/(N_{\text{tot}} - N))$, where N_{tot} is the total number of e -foldings; the parameter r turns out to be proportional to $(n-1)^{2(p+1)/(p+2)}$. Therefore,

$$\frac{\Delta(n-1)}{n-1} = \frac{p+2}{2(p+1)} \frac{\Delta r}{r} = -\frac{\Delta N}{N_{\text{tot}} - N}. \quad (35)$$

Uncertainties in the spectral index can be sizeable if N_{tot} is close to N , but the theoretical errors in r are expected to be suppressed for small r .

The three classes categorized by the relationship between the slow-roll parameters as $-\epsilon < \eta \leq \epsilon$ (large-field), $\eta \leq -\epsilon$ (small-field, linear), and $0 < \epsilon < \eta$ (hybrid), cover the entire $r - n$ plane and are in that sense complete (at least at first order in the slow roll parameters). Figure 1 [24] shows the $r - n$ plane divided into regions representing the large field, small-field and hybrid cases. Figure 2 [25] shows a “zoo plot” of the particular potentials considered here plotted on the $n - \log r$ plane, along with projected errors from forthcoming experiments. For a given choice of potential of the form

$$V(\phi) = \Lambda^4 f\left(\frac{\phi}{\mu}\right), \quad (36)$$

the parameter Λ is generally fixed by CMB normalization, leaving the mass scale μ and the number of e -folds N as free parameters. For some choices of potential, for example $V \propto \exp(\phi/\mu)$ or $V \propto 1 - (\phi/\mu)^2$, the spectral index n varies as a function of μ . These models therefore appear for fixed N as lines on the zoo plot. The inclusion of the uncertainty in N results in a broadening of the line. For other choices of potential, for example $V \propto 1 - (\phi/\mu)^p$ with $p > 2$, the spectral index is independent of μ , and each choice of p describes a point on the

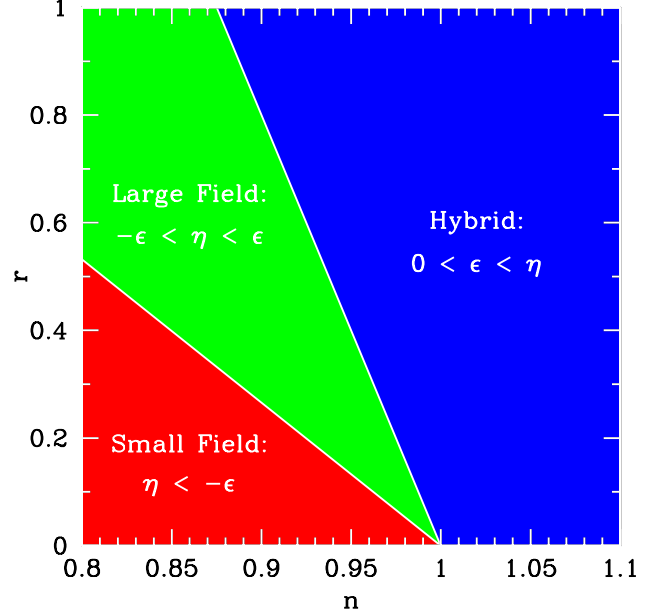


FIG. 1: Regions in the $r - n$ plane corresponding to “large field”, “small field”, and “hybrid” models.

zoo plot for fixed N . The uncertainty in N turns each of these points into lines, which smear together into a continuous region in Fig. 2. Note that even if we include all of these uncertainties, the different classes of potential do not have significant overlap on the zoo plot, and it is therefore possible to distinguish one from another observationally. Furthermore, for a given choice of potential, the uncertainties in r and n arising from the uncertainty in N are generally strongly correlated. This correlation will be apparent in the flow analysis presented below. Finally, for particular choices of potential such as the exponential potential, inflation formally continues forever and the uncertainty due to N vanishes altogether, so there is no “smearing” of the line on the zoo plot.

IV. FLOW EQUATIONS

In this section we describe the flow equations which are a useful tool to quantify the theoretical errors in the inflationary observables due to our ignorance about of the number of e -foldings.

We have defined the slow roll parameters ϵ and η in terms of the Hubble parameter $H(\phi)$ as

$$\begin{aligned} \epsilon &\equiv \frac{m_{\text{Pl}}^2}{4\pi} \left(\frac{H'(\phi)}{H(\phi)} \right)^2, \\ \eta(\phi) &\equiv \frac{m_{\text{Pl}}^2}{4\pi} \left(\frac{H''(\phi)}{H(\phi)} \right). \end{aligned} \quad (37)$$

These parameters are simply related to observables $r \simeq 16\epsilon$, and $n - 1 \simeq 4\epsilon - 2\eta$ to first order in slow roll. Taking higher derivatives of H with respect to the field, we can

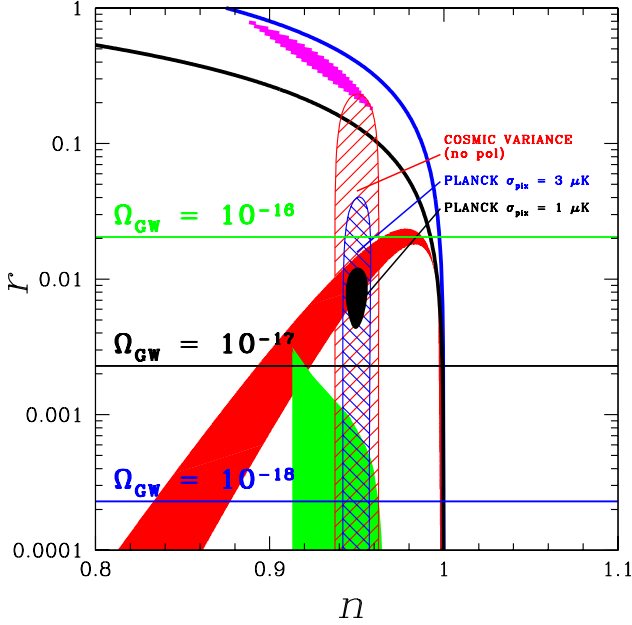


FIG. 2: Predictions of different potentials, including errors due to the uncertainty in N , plotted in the region of $n - \log r$ plane favored by current observation. The model curves, from largest r to smallest, are: $V \propto \exp(\phi/\mu)$ (blue, top), $V \propto \phi^p$ (magenta), $V \propto \phi$ (black), $V \propto 1 - (\phi/\mu)^2$ (red), $V \propto 1 - (\phi/\mu)^p$ ($p > 2$) (green, lowest). The horizontal lines labeled with Ω_{GW} are the expected sensitivities of different proposed configurations of the Big Bang Observer satellite [14]. The hatched error bars are the observational uncertainties for: (a) a cosmic-variance limited temperature-only CMB measurement to $\ell = 1500$ (outer, red), the Planck Surveyor satellite (middle, blue), and a hypothetical CMBPol-like experiment with the same angular resolution as Planck but three times better sensitivity (inner, solid black) [25]. The central value for the error bars shown is arbitrary.

define an infinite hierarchy of slow roll parameters [36]:

$$\sigma \equiv \frac{m_{\text{Pl}}}{\pi} \left[\frac{1}{2} \left(\frac{H''}{H} \right) - \left(\frac{H'}{H} \right)^2 \right],$$

$$\ell \lambda_H \equiv \left(\frac{m_{\text{Pl}}^2}{4\pi} \right)^\ell \frac{(H')^{\ell-1}}{H^\ell} \frac{d^{(\ell+1)}H}{d\phi^{(\ell+1)}}. \quad (38)$$

Here we have chosen the parameter $\sigma \equiv 2\eta - 4\epsilon \simeq n - 1$ to make comparison with observation convenient.

For our purposes, it is convenient to use N as the measure of time during inflation. As above, we take t_e and ϕ_e to be the time and field value at end of inflation. Therefore, N is defined as the number of e -folds before the end of inflation, and increases as one goes *backward* in time ($dt > 0 \Rightarrow dN < 0$):

$$\frac{d}{dN} = \frac{d}{d \ln a} = \frac{m_{\text{Pl}}}{2\sqrt{\pi}} \sqrt{\epsilon} \frac{d}{d\phi}, \quad (39)$$

where we have chosen the sign convention that $\sqrt{\epsilon}$ has

the same sign as $H'(\phi)$:

$$\sqrt{\epsilon} \equiv + \frac{m_{\text{Pl}}}{2\sqrt{\pi}} \frac{H'}{H}. \quad (40)$$

Then ϵ itself can be expressed in terms of H and N simply as,

$$\frac{1}{H} \frac{dH}{dN} = \epsilon. \quad (41)$$

Similarly, the evolution of the higher order parameters during inflation is determined by a set of “flow” equations [17, 18, 19],

$$\begin{aligned} \frac{d\epsilon}{dN} &= \epsilon(\sigma + 2\epsilon), \\ \frac{d\sigma}{dN} &= -5\epsilon\sigma - 12\epsilon^2 + 2(\ell^2 \lambda_H), \\ \frac{d(\ell \lambda_H)}{dN} &= \left[\frac{\ell-1}{2} \sigma + (\ell-2)\epsilon \right] (\ell \lambda_H) + \ell+1 \lambda_H. \end{aligned} \quad (42)$$

The derivative of a slow roll parameter at a given order is higher order in slow roll. At the lowest order, this set of equations properly expressed in terms of observables reproduce equations (2).

A boundary condition can be specified at any point in the inflationary evolution by selecting a set of parameters $\epsilon, \sigma, \ell^2 \lambda_H, \dots$ for a given value of N . This is sufficient to specify a “path” in the inflationary parameter space that specifies the evolution of the observables in terms of the number of e -foldings. Taken to infinite order, this set of equations completely specifies how a shift in the number of e -foldings is reflected in a shift of the slow roll parameters and, therefore, of the observables. Furthermore, such a quantification is exact, with no assumption of slow roll necessary. In practice, we must truncate the expansion at finite order by assuming that the $\ell \lambda_H$ are all zero above some fixed value of ℓ .

Once we obtain a solution to the flow equations $[\epsilon(N), \sigma(N), \ell \lambda_H(N)]$, we can calculate the predicted values of the tensor/scalar ratio r , the spectral index n , and the “running” of the spectral index $dn/d\ln k$ and how they change upon shifting the number of e -foldings by ΔN . To lowest order, the relationship between the slow roll parameters and the observables is especially simple: $r = 16\epsilon$, $n - 1 = \sigma$, and $dn/d\ln k = 0$. To second order in slow roll, the observables are given by [36, 37],

$$r = 16\epsilon [1 - C(\sigma + 2\epsilon)], \quad (43)$$

for the tensor/scalar ratio, and

$$n - 1 = \sigma - (5 - 3C)\epsilon^2 - \frac{1}{4}(3 - 5C)\sigma\epsilon + \frac{1}{2}(3 - C)(\ell^2 \lambda_H) \quad (44)$$

for the spectral index. The constant $C \equiv 4(\ln 2 + \gamma) - 5 = 0.0814514$, where $\gamma \simeq 0.577$ is Euler’s constant. Derivatives with respect to wavenumber k can be expressed in terms of derivatives with respect to N as [38]

$$\frac{d}{dN} = -(1 - \epsilon) \frac{d}{d\ln k}, \quad (45)$$

The scale dependence of n is then given by the simple expression

$$\frac{dn}{d \ln k} = - \left(\frac{1}{1 - \epsilon} \right) \frac{dn}{dN}, \quad (46)$$

which can be evaluated by using Eq. (44) and the flow equations.

It is straightforward to use the flow equations to obtain lowest-order estimates of the expected theoretical errors Δr and Δn in the predictions for r and n by adopting the simple approximation

$$\begin{aligned} \Delta r &\sim \frac{dr}{dN} \Delta N \\ \Delta n &\sim \frac{dn}{dN} \Delta N, \end{aligned} \quad (47)$$

where

$$\begin{aligned} \frac{dr}{dN} &\simeq 16 \frac{d\epsilon}{dN} = 16\epsilon(\sigma + 2\epsilon) \\ &= r[(n-1) + (r/8)], \end{aligned} \quad (48)$$

and

$$\begin{aligned} \frac{dn}{dN} &\simeq \frac{d\sigma}{dN} = -5\epsilon\sigma - 12\epsilon^2 + 2(^2\lambda_H) \\ &= -\frac{5}{16}r(n-1) - \frac{3}{32}r^2 + 2(^2\lambda_H). \end{aligned} \quad (49)$$

We then have estimates for the uncertainties Δr and Δn in terms of the uncertainty in the number of e -folds ΔN :

$$\begin{aligned} \frac{\Delta r}{r} &\sim [(n-1) + (r/8)] (\Delta N) \\ \frac{\Delta n}{n-1} &\sim \left[\frac{5}{16}r + \frac{3}{32} \frac{r^2}{n-1} \right] (\Delta N), \end{aligned} \quad (50)$$

where we have taken $^2\lambda_H \simeq 0$. Figure 3 shows the error estimates from Eq. (50) as a function of r and n . These estimates indicate that the theoretical errors in n and r can be substantial, depending on where the model lives in the r - n plane. If we take the region roughly favored by current observation, $r < 0.1$ and $|n-1| < 0.1$, we have upper bounds on the errors of order

$$\begin{aligned} \frac{\Delta r}{r} &\leq 1 \\ \frac{\Delta n}{|n-1|} &\leq 1, \end{aligned} \quad (51)$$

where these bounds are saturated for $r \sim 0.1$, $|n-1| \sim 0.1$. Note in particular that, for $n-1 \sim 0.1$, the fractional error in r is largely *independent* of the value of r . The fractional errors $\Delta r/r$ and $\Delta n/|n-1|$ are first order in slow roll. The absolute error Δn is second order in slow roll, and since

$$\Delta n \propto \frac{dn}{d \ln k}, \quad (52)$$

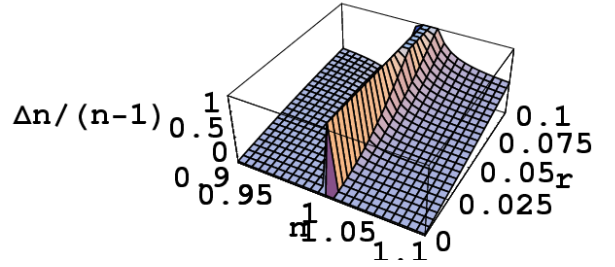
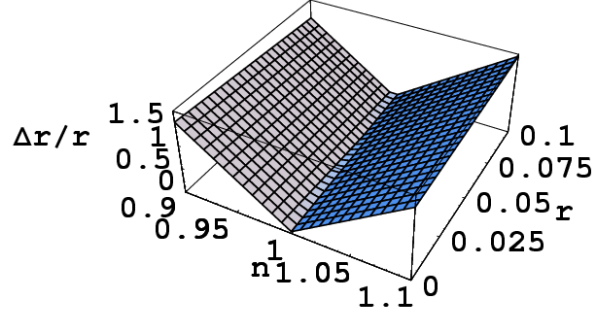


FIG. 3: Lowest order estimates (50) of the theoretical errors $\Delta r/r$ (top) and Δn (bottom) as functions of n and r , assuming $\Delta N = 14$.

we expect substantial absolute error in the spectral index only in models which also predict a relatively large running $dn/d \ln k$. These estimates indicate that the theoretical errors in the inflationary observables can be significant compared to the expected accuracy of future observational constraints. Note that for a single-parameter set of models such as the large-field case (27), there exists an N -independent relation between r and n . Therefore the errors in the parameters are highly correlated. Such models, as we have seen, are falsifiable by observation. Such a simple relation between the observables will not exist for models described by a larger number of parameters. In the next section, we present the results of a Monte Carlo analysis which extends these estimates to higher order in slow roll, effectively increasing the dimensionality of the parameter space describing the potentials.

V. MONTE CARLO ESTIMATE OF THEORETICAL ERRORS

In Sec. IV we derived an analytical estimate of the theoretical errors in the observables n and r to lowest order in slow roll of

$$\frac{\Delta r}{r} \leq 1$$

$$\frac{\Delta n}{|n - 1|} \leq 1 \quad (53)$$

While higher-order analogs of Eq. (50) are in principle possible to derive using the flow equations, a comprehensive investigation of the effect of higher-order terms in slow roll is best accomplished using numerical techniques. In this section, we discuss the results of using a Monte Carlo evaluation of the flow equations to determine the errors $\Delta r/r$ and $\Delta n/|n - 1|$ for a large ensemble of inflationary models.

Monte Carlo evaluation of the flow equations, introduced in Ref. [17], has become a standard technique for investigating the inflationary model space. The principle is straightforward: since the flow equations (42) are first order differential equations, the selection of a point in the slow roll parameter space $\{\epsilon, \eta, {}^2\lambda_H, \dots\}$ serves to completely specify the evolution of a particular model in the space of slow roll parameters. For a model specified in this way, there is a straightforward procedure for determining its observable predictions, that is, the values of r , $n - 1$, and $dn/d\ln k$ a fixed number N e-folds before the end of inflation. The algorithm for a single model is as follows:

- Select a point in the parameter space $\epsilon, \eta, {}^l\lambda_H$.
- Evolve forward in time ($dN < 0$) until either (a) inflation ends, or (b) the evolution reaches a late-time fixed point.
- If the evolution reaches a late-time fixed point, calculate the observables r , $n - 1$, and $dn/d\ln k$ at this point.
- If inflation ends, evaluate the flow equations backward N e-folds from the end of inflation. Calculate the observable parameters at this point.

The end of inflation is given by the condition $\epsilon = 1$. In principle, it is possible to carry out this program exactly, with no assumptions made about the convergence of the hierarchy of slow roll parameters. In practice, the series of flow equations (42) must be truncated at some finite order and evaluated numerically. The calculations presented here are performed to eighth order in slow roll.¹ In effect, we are expanding our model space from the set of single-parameter potentials considered in Sec. III to consider potentials with eight free parameters describing their shape [39].

We wish to determine how the uncertainty in the total number of e-folds N translates into uncertainties in the observable parameters r and n . For models which reach a late-time attractor $r = 0$, $n > 1$ in the flow

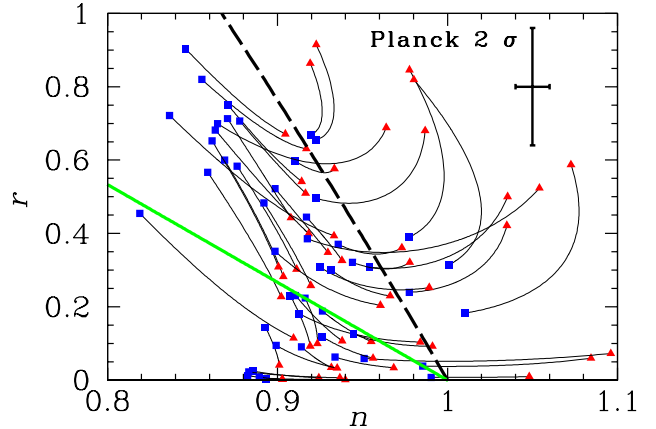


FIG. 4: Flow from $N = 46$ (blue squares) to $N = 60$ (red triangles) for an ensemble of fifty models generated via flow Monte Carlo, plotted in the n - r plane. The path traced by the flow indicates the level of theoretical uncertainty induced by the uncertainty ΔN . The diagonal lines indicate the boundaries between small-field and large-field (green, solid) and large-field and hybrid (black, dashed). Models can “shift” class from $N = 46$ to $N = 60$. The error bar at top right shows projected 2σ measurement uncertainties in n and r for the Planck satellite. The central value for the error bar shown is arbitrary.

space, the answer is trivial: since the observables are evaluated at a fixed point in the flow space, the shift in the observables with N by definition vanishes, and the theoretical uncertainty is in this sense negligible.² We therefore concentrate on models dubbed “nontrivial” in the language of Ref. [17], that is models for which the dynamics carry the evolution through $\epsilon = 1$ and inflation naturally ends after a finite number of e-folds. For a given solution to the flow equations, it is simple to evaluate the effect of moving along the “path” in flow space from $N = 46$ to $N = 60$. (Ref. [40] contains an interesting analytic analysis of the dynamics of paths in the space of flow parameters.)

Figures 4, 5 and 6 illustrate the effect of shifting the number of e-folds in the space of the observables r , n , and $dn/d\ln k$. We see that the effect of the theoretical error in N on the values of the observables is substantial, and at least qualitatively consistent with our rough estimate (50) and with our previous discussion for large and small field models. For large field models and for moderate value of $(1 - n)$ and r , for which the first order approximations hold, we see that the errors increase respectively with $(1 - n)$ and r . Moving towards larger values of these parameters implies a substantial role played by higher or-

¹ The reader is referred to Ref. [17] for a more detailed discussion of the procedure used to stochastically evaluate the flow equations.

² A more realistic hybrid-type model displaying this dynamics will likely be more complex, since the field may not yet have settled into the attractor solution at the appropriate point for calculating cosmological observables. Such a situation is highly model-dependent, and we do not consider it further here.

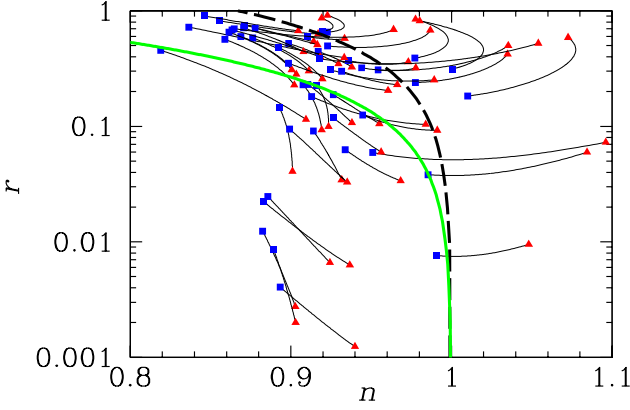


FIG. 5: Flow from $N = 46$ (blue squares) to $N = 60$ (red triangles) for an ensemble of fifty models generated via flow Monte Carlo, plotted in the n - $\log r$ plane, showing the behavior for small r .

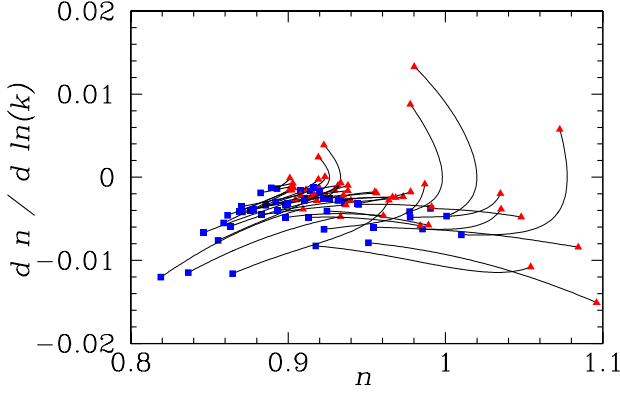


FIG. 6: Flow from $N = 46$ (blue squares) to $N = 60$ (red triangles) for an ensemble of fifty models generated via flow Monte Carlo, plotted in the n - $dn/d \ln k$ plane.

der corrections and errors can be very sizable. For small field models, we observe large displacements along the $(n - 1)$ -axis, but small ones along the r -axis.

We can also see from Fig. 4 that the lowest-order classification of models into small field, large field, and hybrid breaks down when higher order corrections to the dynamics are included. Models which fall into the large-field region at $N = 46$ can evolve into the small-field region at $N = 60$, a behavior which was noted in Ref. [41].

To obtain a more quantitative understanding of the theoretical error in the observables induced by the uncertainty ΔN , we generate an ensemble of models using the flow equations and calculate the observables at $N = 60$, denoted r_{60} and n_{60} , and at $N = 46$, denoted r_{46} and n_{46} . We retain only models which lie close to the region observationally favored by WMAP, $0.9 < n_{60} < 1.1$, and we retain only models with a non-negligible tensor amplitude, $r_{60} > 0.001$. For each model generated by the

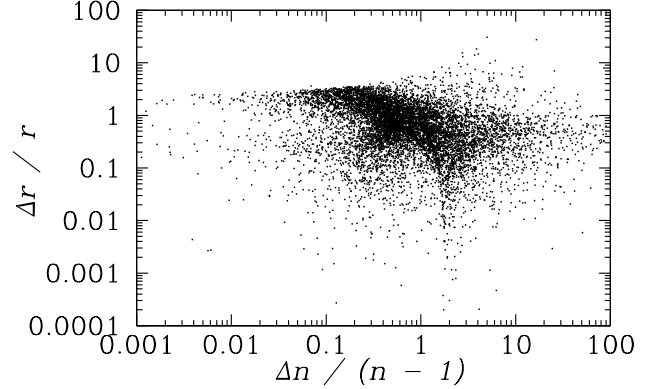


FIG. 7: Theoretical uncertainties Δn and $\Delta r/r$ calculated for an ensemble of 10,000 models with $0.9 < n_{60} < 1.1$ and $r_{60} > 0.001$. The models cluster strongly in the region $\Delta r/r \sim 0.1 - 1$ and $\Delta n/|n - 1| \sim 0.1 - 1$, consistent with the lowest-order estimate (50).

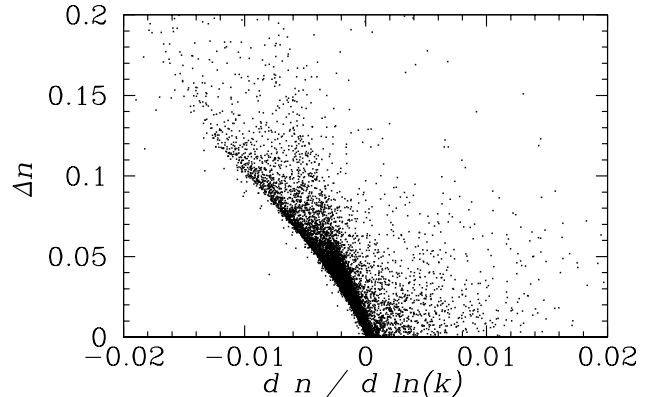


FIG. 8: The absolute uncertainty in the spectral index Δn plotted versus the running $dn/d \ln k$. As expected, the uncertainty in the spectral index becomes large for models which predict significant running.

Monte Carlo, we then assign uncertainties in r and n as:

$$\frac{\Delta r}{r} = \left| \frac{r_{60} - r_{46}}{r_{60}} \right|, \quad (54)$$

and

$$\frac{\Delta n}{|n - 1|} = \left| \frac{n_{60} - n_{46}}{n_{60} - 1} \right|. \quad (55)$$

Figure 7 shows the above uncertainties calculated for an ensemble of 10,000 models. We see that the estimates $\Delta r/r \sim \Delta n/|n - 1| \sim 1$ are robust even when calculated to higher order. Figure 8 shows the uncertainty Δn plotted against the running of the spectral index $dn/d \ln k$, showing the expected strong correlation between the error Δn and the running.

VI. CONCLUSIONS

We have considered the implications of the uncertainty in the reheat temperature on the observable predictions of inflation. The most convenient parameters for discriminating among inflation models are the tensor/scalar ratio r and the scalar spectral index n . These parameters are simply related to the inflationary slow roll parameters ϵ and η , and this correspondence can be generalized to higher order in the slow roll expansion through the inflationary flow equations. The uncertainty in the reheat temperature corresponds to uncertainty in the number of e -folds of expansion N during the inflationary epoch,

$$N \simeq 60 + \frac{1}{6} \ln(-n_T) + \frac{1}{3} \ln(T_{\text{RH}}/10^{16} \text{ GeV}) - \frac{1}{3} \ln \gamma, \quad (56)$$

where T_{RH} is the reheating temperature, γ is the ratio of the entropy per comoving volume today to that after reheating. If we assume γ is negligible, the large uncertainty in the reheat temperature corresponds to an uncertainty in the number of e -folds $\Delta N \sim 14$. This can be related to a theoretical uncertainty in the observable parameters r and n to lowest order by using the flow relations

$$\begin{aligned} \frac{\Delta r}{r} &\sim [(n-1) + (r/8)] (\Delta N), \\ \frac{\Delta n}{n-1} &\sim \left[\frac{5}{16} r + \frac{3}{32} \frac{r^2}{n-1} \right] (\Delta N). \end{aligned} \quad (57)$$

For r and n in the region favored by current observational constraints, these errors can in principle be large, $\Delta r/r \sim 0.1 - 1$, and $\Delta n/|n-1| \sim 0.1 - 1$. We also analyze the expected theoretical uncertainty in the inflationary observables by Monte Carlo evaluation of the inflationary flow equations to eighth order in slow roll, and find results consistent with the lowest-order estimate above, but with considerable scatter in the models. We have numerically checked that these errors increase ap-

proximately linearly with ΔN as suggested by the lowest-order estimate. The absolute error in the spectral index can be compared with the expected 2σ uncertainty in the spectral index from the Planck satellite, $\Delta n \sim 0.01$, and is seen to be typically of the same order.

We conclude that the theoretical uncertainties in the inflationary observables are generically of the order of or larger than the projected uncertainties in future precision measurements of the Cosmic Microwave Background, and represent a significant challenge for the program of using observation to distinguish among the many different candidate models for inflation in the early universe. While the dependence of the inflationary observables on the number of e -folds N is certainly well known (and was, for example, taken into account by WHK in Refs. [17, 25]), it has not been emphasized as the dominant source of theoretical error in the predictions of inflation. The error induced by the uncertainty in the reheat temperature and/or in the amount of entropy release after inflation (and thus in N) is typically much larger than errors in the quantities r and n due to using the slow roll approximation to calculate the primordial power spectrum, a subject which has received considerable attention in the literature [19, 42, 43, 44, 45, 46]. The expected uncertainties for any *particular* choice of potential are model-dependent: it will certainly still be possible to rule out models of inflation with future precision data. However, it will be necessary to move beyond the simple lowest-order description of the inflationary parameter space which has so far been good enough.

Acknowledgments

AR is on leave of absence from INFN Padova, Italy. We thank Brian Powell for work on an upgraded flow code. WHK is supported in part by the National Science Foundation under grant NSF-PHY-0456777.

[1] For reviews, see D. H. Lyth and A. Riotto, Phys. Rept. **314**, 1 (1999); W. H. Kinney, arXiv:astro-ph/0301448.

[2] A. A. Starobinsky, JETP Lett. **30**, 682 (1979) [Pisma Zh. Eksp. Teor. Fiz. **30**, 719 (1979)].

[3] V. F. Mukhanov and G. V. Chibisov, JETP Lett. **33**, 532 (1981).

[4] J. M. Bardeen, P. J. Steinhardt, and M. S. Turner, Phys. Rev. D **28**, 679 (1983).

[5] C. L. Bennett *et al.* Astrophys. J. **464**, L1 (1996).

[6] K. M. Gorski *et al.* Astrophys. J. **464**, L11 (1996).

[7] C. L. Bennett *et al.*, Astrophys. J. Suppl. **148**, 1 (2003).

[8] H. V. Peiris *et al.*, Astrophys. J. Suppl. **148**, 213 (2003); W. H. Kinney, E. W. Kolb, A. Melchiorri and A. Riotto, Phys. Rev. D **69**, 103516 (2004).

[9] See <http://www.rssd.esa.int/index.php?project=PLANCK>.

[10] See www.mssl.ucl.ac.uk/www_astro/submm/CMBpol1.html.

[11] See <http://astro.uchicago.edu/spt/>.

[12] M. Kaplinghat, L. Knox and Y. S. Song, Phys. Rev. Lett. **91**, 241301 (2003).

[13] M. Kesden, A. Cooray and M. Kamionkowski, Phys. Rev. Lett. **89** (2002) 011304; L. Knox and Y.-Song, Phys. Rev. Lett. **89** (2002) 011303.

[14] S. Phinney, et al., “The Big Bang Observer: Direct detection of gravitational waves from the birth of the universe to the present,” NASA mission concept study (2005).

[15] B. de Carlos, J. A. Casas, F. Quevedo and E. Roulet, Phys. Lett. B **318**, 447 (1993).

[16] A. R. Liddle and S. M. Leach, Phys. Rev. D **68**, 103503 (2003).

[17] W. H. Kinney, Phys. Rev. D **66**, 083508 (2002).

[18] M. B. Hoffman and M. S. Turner, Phys. Rev. D **64**, 023506 (2001).

- [19] D. J. Schwarz, C. A. Terrero-Escalante, and A. .A. Garcia, Phys. Lett. **B517**, 243 (2001).
- [20] L. P. Grishchuk and Yu. V. Sidorav, in *Fourth Seminar on Quantum Gravity*, eds M. A. Markov, V. A. Berezin and V. P. Frolov (World Scientific, Singapore, 1988).
- [21] A. G. Muslimov, Class. Quant. Grav. **7**, 231 (1990).
- [22] D. S. Salopek and J. R. Bond, Phys. Rev. D **42**, 3936 (1990).
- [23] J. E. Lidsey *et al.*, Rev. Mod. Phys. **69**, 373 (1997), astro-ph/9508078.
- [24] S. Dodelson, W. H. Kinney, and E. W. Kolb, Phys. Rev. D **56**, 3207 (1997), astro-ph/9702166.
- [25] W. H. Kinney, Phys. Rev. D **58**, 123506 (1998).
- [26] A. D. Linde, Phys. Lett. **129B**, 177 (1983).
- [27] A. D. Linde, Phys. Lett. **B108** 389, 1982.
- [28] A. Albrecht and P. J. Steinhardt, Phys. Rev. Lett **48**, 1220 (1982).
- [29] K. Freese, J. Frieman, and A. Olinto, Phys. Rev. Lett **65**, 3233 (1990).
- [30] A. D. Linde, Phys. Lett. **259B**, 38 (1991).
- [31] A. D. Linde, Phys. Rev. D **49**, 748 (1994).
- [32] E. J. Copeland, A. R. Liddle, D. H. Lyth, E. D. Stewart, and D. Wands, Phys. Rev. D **49**, 6410 (1994); A. D. Linde and A. Riotto, Phys. Rev. D **56**, 1841 (1997).
- [33] J. D. Barrow and A. R. Liddle, Phys. Rev. D **47**, R5219 (1993).
- [34] W. H. Kinney and A. Riotto, Astropart. Phys. **10**, 387 (1999).
- [35] W. H. Kinney and A. Riotto, Phys. Lett. **435B**, 272 (1998).
- [36] A. R. Liddle, P. Parsons, and J. D. Barrow, Phys. Rev. D **50**, 7222 (1994).
- [37] E. D. Stewart and D. H. Lyth, Phys. Lett. **302B**, 171 (1993).
- [38] A. R. Liddle. and M. S. Turner, Phys. Rev. D **50**, 758 (1994).
- [39] A. R. Liddle, Phys. Rev. D **68**, 103504 (2003) [arXiv:astro-ph/0307286].
- [40] S. Chongchitnan and G. Efstathiou, arXiv:astro-ph/0508355.
- [41] D. J. Schwarz and C. A. Terrero-Escalante, JCAP **0408**, 003 (2004) [arXiv:hep-ph/0403129].
- [42] J. O. Gong and E. D. Stewart, Phys. Lett. B **510**, 1 (2001) [arXiv:astro-ph/0101225].
- [43] S. Habib, K. Heitmann, G. Jungman and C. Molina-Paris, Phys. Rev. Lett. **89**, 281301 (2002) [arXiv:astro-ph/0208443].
- [44] S. Habib, A. Heinen, K. Heitmann, G. Jungman and C. Molina-Paris, Phys. Rev. D **70**, 083507 (2004) [arXiv:astro-ph/0406134].
- [45] R. Casadio, F. Finelli, M. Luzzi and G. Venturi, Phys. Rev. D **71**, 043517 (2005) [arXiv:gr-qc/0410092].
- [46] A. Makarov, arXiv:astro-ph/0506326.